Title

Transparent, Compliant 3D Mesostructures for Precise Evaluation of Mechanical Characteristics of Organoids.

Journal

Advanced Materials, 33(25)

Authors

Ryu, Hanjun
Park, Yoonseok
Luan, Haiwen
et al.

Publication Date

2021-06-01

DOI

10.1002/adma.202100026

Peer reviewed

HHS Public Access

Author manuscript

Adv Mater. Author manuscript; available in PMC 2022 June 01.

Published in final edited form as:

Adv Mater. 2021 June ; 33(25): e2100026. doi:10.1002/adma.202100026.

Transparent, compliant 3D mesostructures for precise evaluation of mechanical characteristics of organoids

Hanjun Ryu,
Center for Bio-Integrated Electronics, Querrey Simpson Institute for Bioelectronics, Northwestern University, Evanston, IL 60208, USA; School of Advanced Materials Science and Engineering, Sungkyunkwan University (SKKU), Suwon 16419, Republic of Korea

Yoonseok Park,
Center for Bio-Integrated Electronics, Querrey Simpson Institute for Bioelectronics, Northwestern University, Evanston, IL 60208, USA

Haiwen Luan,
Center for Bio-Integrated Electronics, Querrey Simpson Institute for Bioelectronics, Northwestern University, Evanston, IL 60208, USA

Gokhan Dalgin,
Section of Adult and Pediatric Endocrinology, Diabetes and Metabolism, Kovler Diabetes Center, The University of Chicago, IL 60637

Kira Jeffris,
Department of Mechanical and Industrial Engineering, University of Illinois at Chicago, Chicago, IL 60607

Hong-Joon Yoon,
Center for Bio-Integrated Electronics, Querrey Simpson Institute for Bioelectronics, Northwestern University, Evanston, IL 60208, USA; School of Advanced Materials Science and Engineering, Sungkyunkwan University (SKKU), Suwon 16419, Republic of Korea

Ted S. Chung,
Department of Biomedical Engineering, Northwestern University, Evanston, IL 60208, USA; Center for Bio-Integrated Electronics, Northwestern University, Evanston, IL 60208, USA

Jong Uk Kim,
School of Chemical Engineering, Sungkyunkwan University (SKKU), Suwon 16419, Republic of Korea

Sung Soo Kwak,
Center for Bio-Integrated Electronics, Querrey Simpson Institute for Bioelectronics, Northwestern University, Evanston, IL 60208, USA; School of Advanced Materials Science and Engineering, Sungkyunkwan University (SKKU), Suwon 16419, Republic of Korea

Geumbee Lee,

jdfinan@uic.edu; jrogers@northwestern.edu.

Supporting Information

Supporting Information is available from the Wiley Online Library or from the author.

Center for Bio-Integrated Electronics, Querrey Simpson Institute for Bioelectronics, Northwestern University, Evanston, IL 60208, USA

Hyoyoung Jeong,
Center for Bio-Integrated Electronics, Querrey Simpson Institute for Bioelectronics, Northwestern University, Evanston, IL 60208, USA

Jihye Kim,
Center for Bio-Integrated Electronics, Querrey Simpson Institute for Bioelectronics, Northwestern University, Evanston, IL 60208, USA; School of Advanced Materials Science and Engineering, Sungkyunkwan University (SKKU), Suwon 16419, Republic of Korea

Wubin Bai,
Department of Applied Physical Sciences, University of North Carolina at Chapel Hill, Chapel Hill, NC, 27599, USA

Joohee Kim,
Center for Bio-Integrated Electronics, Querrey Simpson Institute for Bioelectronics, Northwestern University, Evanston, IL 60208, USA

Yei Hwan Jung,
Department of Electronic Engineering Hanyang University, Seoul 04763, Republic of Korea

Andrew K. Tryba,
Section of Pediatric Neurology, Department of Pediatrics, The University of Chicago, IL, 60637, USA

Joseph W. Song,
Department of Biomedical Engineering, Northwestern University, Evanston, IL 60208, USA; Center for Bio-Integrated Electronics, Northwestern University, Evanston, IL 60208, USA

Yonggang Huang,
Department of Mechanical Engineering, Northwestern University, Evanston, IL 60208, USA; Department of Civil and Environmental Engineering, Northwestern University, Evanston, IL 60208, USA; Department of Materials Science and Engineering, Northwestern University, Evanston, IL 60208, USA; Center for Bio-Integrated Electronics, Querrey Simpson Institute for Bioelectronics, Northwestern University, Evanston, IL 60208, USA

Louis H. Philipson,
Department of Medicine and Kovler Diabetes Center, The University of Chicago, IL 60637

John D. Finan,
Department of Mechanical and Industrial Engineering, University of Illinois at Chicago, Chicago, IL 60607

John A. Rogers
Center for Bio-Integrated Electronics, Querrey Simpson Institute for Bioelectronics, Northwestern University, Evanston, IL 60208, USA; Department of Mechanical Engineering, Northwestern University, Evanston, IL 60208, USA; Department of Materials Science and Engineering, Northwestern University, Evanston, IL 60208, USA; Department of Biomedical Engineering, Northwestern University, Evanston, IL 60208, USA; Department of Chemistry, Northwestern

University, Evanston, IL 60208, USA; Department of Electrical and Computer Engineering, Northwestern University, Evanston, IL 60208, USA; Departments of Neurological Surgery, Feinberg School of Medicine, Northwestern University, Chicago, IL 60611, USA

Abstract

Recently developed methods for transforming two-dimensional (2D) patterns of thin film materials into 3D mesostructures create many interesting opportunities in microsystems design. A growing area of interest is in multifunctional thermal, electrical, chemical and optical interfaces to biological tissues, particularly 3D multicellular, millimeter-scale constructs such as spheroids, assembloids and organoids. This paper presents examples of 3D mechanical interfaces, in which thin ribbons of parylene-C form the basis of transparent, highly compliant frameworks that can be reversibly opened and closed to capture, envelop and mechanically restrain fragile 3D tissues in a gentle, non-destructive manner, for precise measurements of viscoelastic properties using techniques in nanoindentation. Finite element analysis serves as a design tool to guide selection of geometries and material parameters for shape-matching 3D architectures tailored to organoids of interest. These computational approaches also quantitate all aspects of deformations during the processes of opening and closing the structures and of forces imparted by them onto the surfaces of enclosed soft tissues. Studies by nanoindentation show effective Young's moduli in the range from 1.5 to 2.5 kPa depending on the age of the organoid. This collection of results suggest broad utility in non-invasive mechanical measurements of millimeter-scale, soft biological tissues.

Graphical Abstract

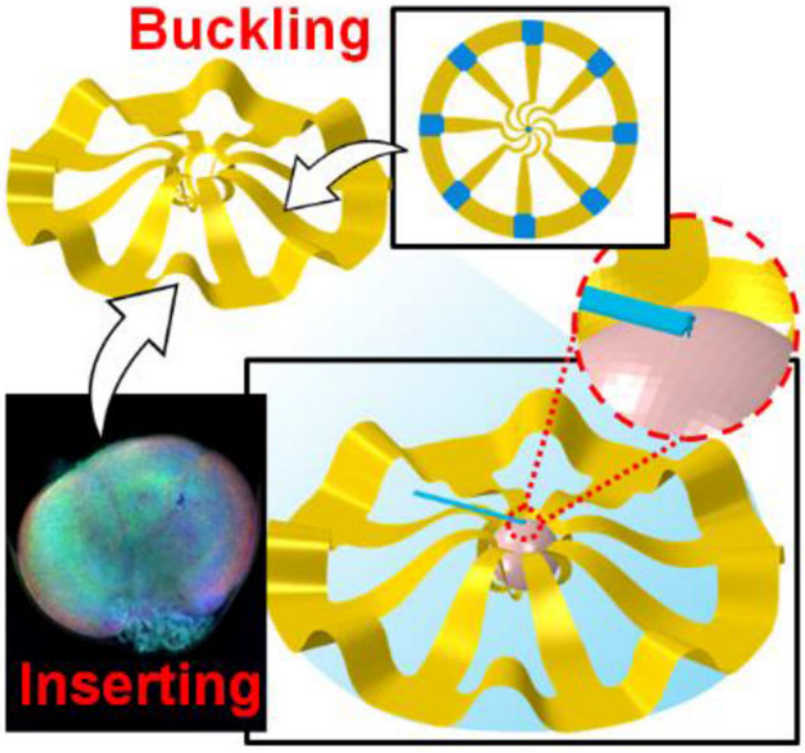

Abstract

3D mesostructures design to mechanically and reversibly constrain organoids. Finite element analysis selects 3D layouts to grasp organoids with minimal force, and calcein-AM/PI cell viability assays do not detect damage to the tissues. Nanoindentation can be applied directly to organoids for accurate and repeated measurements of force/displacement data. Changes in mechanical characteristics by drugs highlight responses to the chemical environment.

Keywords

3D mesostructures; Mechanical buckling; Finite element analysis; Young's modulus; Organoid

1. Introduction

3D mesostructures are of widespread interest because, by comparison to conventional 2D counterparts, they offer expanded and enhanced functional possibilities in areas ranging from biomedical devices[1–7], electronic devices[8–13], and sensors[14–17]. Although fabrication techniques based on 3D printing[18–20], self-rolling[21–23] and origami/kirigami[24–26] offer utility in this context, each has some set of limitations in materials compatibility, structural diversity, resolution and patterning speed. Alternative schemes based on mechanical assembly begin with formation of 2D thin-film structures using any of a wide variety of sophisticated lithographic approaches applied to the most advanced functional materials. Controlled processes of buckling transform these 2D precursors into open-architecture 3D geometries in a high-speed, parallel fashion with versatility in materials (semiconductors, metals, insulators of both organics and inorganics), layer thicknesses (from millimeters to atomic dimensions), feature sizes (from nanometers to centimeters) and layouts (open or closed architectures of ribbons, beams, membranes and others)[27–30].

These capabilities in materials, devices and 3D assembly methods are highly relevant in the context of biological systems, where 3D design features are ubiquitous. Miniaturized 3D tissue constructs are of particular interest, due to their increasing roles in biological research. Here, human induced pluripotent stem cells grown into 3D cell cultures serve as model systems of vital organs, from the heart to the brain, the spinal cord, the liver, the gut and others. Brain tissues of such types, referred to as cerebral organoids[31,32], can be used as platforms for studies of neural differentiation, regeneration, communication, development and disease. Recent work demonstrates the ability of 3D constructs, called 3D multifunctional mesoscale frameworks (3D MMFs), to serve as electrical, thermal, optical and chemical interfaces to these systems[55]. Many biological properties and behaviors depend also on mechanical cues and characteristics, at the level of individual cells and collections of them and their interactions with surrounding materials. Relevant effects include aspects of cell formation, functionality, motility, differentiation and others[33]. Cytoskeletal, nuclear, or extracellular matrix (ECM) changes contribute to changes in the Young's modulus of organoids, as indicators of abnormalities and mutations[34,54]. Direct characterization of the mechanical properties with probes such as nanoindenters or tips for atomic force microscopy can, however, be challenging because these structures move freely in cell culture media without positional fixation[35]. Hydrogels can be useful

as concave cavities shape-matched to the organoids[37,38], but their fabrication can be cumbersome[34,36] and they often do not maintain the positions of the organoids during cell culture medium exchange, introduction of drugs or other manipulations. Microwell arrays are capable of separating organoids, but organoids randomly rotate and move in the microwells.

This paper introduces a soft and transparent class of 3D MMF designed to gently envelop and mechanically constrain organoids in ways that facilitate mechanical evaluations without damage. The photolithography-based fabrication process realizes micron thickness and complex 2D precursors with a variety of material options such as parylene-C, polyimide (PI), and more, and can integrate electronic functions[55]. These 3D structures can be reversibly deformed by laterally stretching a thin elastomeric substrate, as a mechanism to open and close around an organoid in a controlled manner. Finite element analysis (FEA) serves as a guide to select 3D layouts that match the geometries of organoids of interest and to grasp them with minimal force. Calcein-AM/propidium iodide (PI) cell viability assays and optical microscopy studies do not detect acute damage to the tissues. Techniques of nanoindentation can be applied directly to organoids while enclosed in these frameworks, for accurate and repeated measurements of force/displacement data. The effective Young's moduli determined from these measurements exhibit dependence on age, indentation depths, indentation speeds. Changes in mechanical characteristics induced by controlled exposure to blebbistatin and ethanol highlight options in studies of responses to the chemical environment. The results suggest broad utility in precise, non-destructive mechanical testing of small-scale biological tissues.

2. Results and Discussion

Figure 1a shows a schematic illustration of a 3D MMF designed for these purposes, and of steps in opening and closing this structure around a cerebral organoid with an approximately spherical shape. The design of the 2D precursor, the bonding sites and the prestrain field are the main factors that determine the 3D geometry; gravity and buoyancy have a negligible effect when the organoid and 3D MMF are immersed in a cell culture medium. Here, the 2D precursor consists of a thin (~ 13 μm) layer of parylene-C (para-xylylene dimer, Specialty Coating Systems Inc., USA) patterned by photolithography and reactive-ion etching (RIE). Electron beam evaporation through a shadow mask forms square pads of Ti/SiO_2 (10/100 nm in thickness) at selected regions on the bottom side of the 2D precursor, to define sites of bonding to a biaxially stretched (30 %) thin (~ 1.2 mm in thickness) substrate of poly(dimethylsiloxane) (PDMS, Sylgard 184, Dow, USA; 20:1). In one example, the 2D precursor includes a radially symmetric collection of eight 'wings' with widths of 170 μm and a section that twists into a curved structure with inner and outer radii of 720 μm ($R_{in,1}$) and 920 μm ($R_{out,1}$), respectively, terminating with a width of 440 μm. The widths of the straight sections increase linearly from 440 μm to 1 mm along a length of 3.8 mm. (See Figure S1, Method, Supporting Information). Allowing the substrate to relax to its unstretched state leads to compressive forces on the 2D precursor at the bonding locations. The result leads to delamination at the non-bonded regions, with translational and rotational motions out of the plane, thereby transforming the system into a 3D structure. The 3D MMF uses a 35 mm cell culture plate (or larger) to contain the cell culture medium. Stretching or

relaxing the substrate opens or closes, respectively, the system to allow for manual insertion or removal of an organoid (Figure 1b; see Figure S2, Supporting Information, Supporting Movie 1). The FEA results demonstrate this process of inserting the organoid into the 3D MMF (see Figure 1c). Figure 1d demonstrates the scalability of the process and the ability to locally open/close individual 3D MMFs in a large array by vertically pressing the bottom elastic substrate of each 3D MMF, fabricated in this case from a 12.5 μm thick substrate of PI (Dupont, USA) using laser manufacturing process to simplify the fabrication process. Currently, the five frameworks is the maximum number possible in a single system due to practical considerations based on the size of the stretchable substrate, the design of the mechanical stretcher, and area of the 2D precursor.

Procedures for forming the cerebral organoids follow protocols by Lancaster (see Figure 1a (iii))[39] using an iPSC line with confirmed expression of pluripotency markers NANOG and OCT4 (see Figure S3 a,b) and ability to differentiate into three germ layers; PAX6 expressing ectoderm, BRA expressing mesoderm, and FOXA2 expressing endoderm (see Figure S3 c–e). The developing organoids show typical morphology (see Figure S3 f–i) and expression of the neural stem cell marker SOX2 and forebrain marker FOXG1 (see Figure S3 j, k).

Figure 2 summarizes essential geometrical and mechanical properties features of several different 3D MMFs. The version with curved wings forms 1) a twisted structure with a peak rotation angle of 40.4 degrees and large convex curvature, and 2) a gradual concave curvature, sequentially, to create an enclosed space in an approximately spherical shape (see Figure 2a). Circular curves drawn within the space defined by the structure, oriented parallel to the substrate, have diameters of 1162, 1420, 1676, 1784, 1770, 1670, 1458, and 1294 μm at heights of 100, 200, 400, 600, 800, 1000, 1200, 1300 μm, respectively, above the substrate (see Figure 2b, Figure S4, Supporting Materials). This twisted design forms a large volume within the structure and a shape accurately tailored for spherical organoids, as differentiated from the less optimal, straight wing design as previously reported. The bending stiffness at the point of the central bonding site is 8.84×10^{-11} N·m^2 (section 1), increasing to 2.46 $\times10^{-10}$ N·m^2 (section 2) and finally to 5.23 $\times10^{-10}$ N·m^2 (section 3) (see Figure 2c). The design with straight wings forms 1) a gradual convex curvature from the central bonding site, 2) a linear region, and 3) a gradual concave curvature to define an approximately conical enclosed space (see Figure 2d). This space is characterized by diameters of 912, 1080, 1278, 1386, 1474, 1588, 1764, and 1906 μm at heights of 100, 200, 400, 600, 800, 1000, 1200, 1300 μm, respectively, above the substrate (see Figure 2e, Figure S4, Supporting Materials). The bending stiffness at the point of the central bonding site is 8.59×10^{-11} N·m^2 (section 1), increasing to 2.79 $\times10^{-10}$ N·m^2 (section 2) and finally to 5.23 $\times10^{-10}$ N·m^2 (section 3), similar to the twisted system (see Figure 2f). Simulations in Figure S5 indicate that the twisted structure fixes a spherical organoid with a diameter of 1.7 mm under a maximum compressive stress of 824 Pa from top to bottom; the straight structure cannot hold the same type of organoid due to insufficient maximum lateral compressive stress (183 Pa) and effects of buoyancy and minute fluid flows, thereby leading to uncontrolled slight motions.

Figure 3 shows the results of FEA for the out-of-plane displacements as well as the distributions of strain and stress for 3D MMFs and enclosed organoids. Design choices here match those of the shapes and sizes of the organoids. Spherical organoids with diameters at least 1.6 mm can fit into cavities defined by 3D structures with maximum heights of 1.5 mm (Figure 3a). According to the results of Figure 3b, the strains that occur in the 3D MMF are less than limits of plastic deformation and fracture of the parylene-C[40]. An organoid with a diameter of 1.6 mm, which is the smallest size that can fit into the 3D MMF, is free from any stress induced by the 3D MMF (see Figure 3b,3c, and Figure S6, Supporting Information). Figure 3d shows an example of an ellipsoidal organoid (a = 0.9 mm, b = 0.9 mm, c = 0.75 mm) with the minimum size for the 3D MMF. The dimensions of this organoid ensure an absence of forced contact with the 3D MMF, such that the strain distribution in the 3D MMF is unaltered and the organoid is free from stresses (see Figure 3e,3f, and Figure S6, Supporting Information). Figure 3g demonstrates the case of insertion of a spherical organoid with a diameter of 1.7 mm, where stresses (up to ~2 kPa in compression) form at the areas of contact (see Figure 3h,3i, and Figure S6, Supporting Information). In general, a 3D MMF can hold an organoid with a diameter up to ~ 0.1 mm larger than the design point without significant deformation and damage[41]. Linear scaling (expansion or contraction) of the 2D framework renders 3D MMFs with different sizes to match requirements (see Figure S7, Supporting Information). For a larger spherical organoid with a diameter of 2.2 mm, a 3D MMF, linearly scaled up by a factor of 2.2/1.7, can hold an organoid with similar strain/stress levels (see Figure 3g–3i, Figure S8, Supporting Information).

Studies of cytotoxicity involve Calcein AM/PI as a stain for viable/dead cells for five different conditions and organoid groups (see Figure 4). Figure 4a shows results of Calcein AM staining of spherical organoids with diameters of ~ 1.7 mm inserted into a 3D MMF with the twisted design. Figure 4b highlights findings associated with PI staining, including cases of i) a positive control (an organoid not in a 3D MMF), ii) a negative control (an organoid exposed to a toxic drug), iii) an organoid one hour after insertion into a 3D MMF followed by removal, iv) an organoid 24 hours after insertion into a 3D MMF followed by removal, v) an organoid after five cycles of insertion and removal from a 3D MMF, and vi) an organoid 24 hours after insertion into a 3D MMF, while still in the 3D MMF. Comparisons of bright-field images before insertion and fluorescence images after show that the organoids remain intact for all insertion conditions with no evidence of fragmentation or rupture (see Figure S9, Supporting Information). The positive control shows mild green and red fluorescence; the negative control shows zero green fluorescent and a high red fluorescence. The cases of (iii), (iv) and (v) show similar levels of green and red fluorescence, consistent with absence of damage (see Figure 4c–e). The ratio of PI and Calcein AM of the negative control is not well defined due to the absence of green pixels. Quantitative real time polymerase chain reaction (qRT-PCR) measures 4 target genes (FOXG1, RBFOX3/NEUN, S100B, TUJ1/TUBB3) and two reference genes (18S, RPL37A) in each of these organoids to quantify changes in gene expression after insertion into 3D MMF. The Control group (n=4) maintains in dishes with 3D MMF but not inserted, and the experimental group (n=3) maintains in 3D MMF for 24 hours. The relative change in expression of each target gene is computed by the delta-delta CT method, and the results show similar tendencies regardless of the reference genes (see Table 1, Table 2, and Table

S1, Supporting Information). FOXG1 is relatively insensitive to insertion; RBFOX3/NEUN significantly increases. The transparency of the 3D MMF (85 % across the visible; see Figure S10, Supporting Information) facilitates these and other forms of optical assays (see Figure 4a(vi),b(vi)).

Figure 5 highlights measurements of mechanical properties of cerebral organoids held in the 3D MMF with the twisted geometry, while immersed in cell culture media. The tip of the nanoindenter (Piuma nanoindenter, Optics 11, Netherlands) establishes contact to the organoid through the exposed top area of the structure. The elastic modulus (E) of the organoid can be derived from application of the Hertz model:[42,43]

$$E = \frac{3\left(1 - \upsilon^2\right)P}{4R^{1/2}h^{3/2}} \quad (1)$$

where υ is Poisson's ratio of the indenter, P is the load, R is the radius of the spherical indenter tip, h is the penetration depth. The effective Young's modulus of the 3D MMF is ~ 10 kPa around the top area, and ~ 7 kPa near the middle wing area. These values are significantly less than those of flat 1, 2, and 4 % agarose gel continuums (see Figure S11, Supporting Information). The force-distance curves collected in this manner have much less noise and exhibit much clearer repulsive force behaviors than those obtained from organoids without constraint (see Figure 5a, Figure S12, Supporting Information). A 171-day aged organoid shows an effective Young's modulus of 2.2 ± 0.1 kPa, consistent with previous AFM studies[34,43–45]. Attempts to measure the Young's modulus of the same organoid on a flat polymer substrate yield values < 1 kPa, limited by poor accuracy in the force-distance data that follows from lateral movements of the organoid during the measurement. Figure 5b shows the effective Young's modulus of organoids with ages from 63 to 171 days. The diameters of the organoids increase with age, from 1.4 to 2.2 mm. The middle-aged organoids (between 60 and 100 days) show effective Young's moduli of 1.5 ~ 2 kPa. Mature organoids (over 100 days) have moduli of 2 ~ 2.5 kPa (see Figure S3 f–i). Data from indentation depths between 3.5 to 12 μm have slightly different types of force-distance curves, with moduli from ~ 1.4 to ~ 2.4 kPa with increasing depth (see Figure 5c)[46]. The effective modulus also depends on indentation speed, changing monotonically from 1.3 to 3.3 kPa for speeds from 1 to 75 μm/s (see Figure 5d)[47].

The open architecture of these 3D MMFs allows direct studies of the effects of drugs on modulus, following from their influence on actin fibers, myosin filaments, and cytoskeletons. Examples reported here include introduction of 10 μM of blebbistatin[48] and 50 mM of ethanol[49], as representative chemistries that reduce and enhance the modulus without significant toxicity (see Figure S13, Supporting Information). Figure 5e presents data that show that the effective Young's modulus decreases from ~ 2.4 kPa to 0.9 kPa after 2-hour exposure to 10 μM of blebbistatin, consistent with expected disruption of myosin contractility and actin polymerization[50]. The effective Young's modulus increases from ~ 2 kPa to 5.5 kPa after 2-hour exposure to 50 mM of EtOH treatment (see Figure 5f), consistent with the promotion of phosphorylation of myosin motor proteins[51,52] and consequent increase in tension in actin fibers[53].

While nanoindentation is the primary assay in this study, many other important and popular assays will be easier to apply to organoids when they are immobilized with a 3D MMF. For example, the widely use patch clamp electrophysiological assay also requires pressing a probe gently against the sample and this is difficult to do when the sample is mobile. Also, high content time series imaging typically involves cycling through locations on the assumption that previously viewed samples will be at the previous viewed location when it is time to view them again. 3D MMFs can position organoids stably and consistently to make these and other similar assays more reliable and easier to apply. Therefore, 3D MMFs are likely to find many powerful applications in the study of brain organoids.

3. Conclusion

In summary, the compliant and transparent 3D MMFs introduced here provide simple but useful function in spatially constraining organoids for purposes of mechanical characterization. Lateral stretching of a thin elastomeric substrate provides a convenient means for opening and closing the structure to facilitate insertion and removal of organoids for testing. A twisted design in the 3D framework yields a highly spherical cavity with dimensions that can be matched precisely to organoids of interest. FEA techniques serve as design tools to allow proper selection of 2D precursor geometries and to minimize mechanical stresses on enclosed organoids. Detailed studies indicate that organoids can be released from these constructs non-destructively. Nevertheless, the possibility that insertion into the 3D MMF might perturb gene expression cannot be excluded at this time. Also, 3D MMF-induced cellular compression can possibly stimulate mechanosensitive pathways that will alter cell behavior. Measurements indicate that organoids of various ages and sizes have different characteristic Young's moduli, and that the depths and speeds of indentation can influence the apparent values, consistent with expectation and prior literature studies. The open architecture designs allow free diffusive and forced convective access to the surfaces of the organoids, as demonstrated through studies of the effects of blebbistatin and ethanol on the mechanical properties. This collection of results suggests that techniques in controlled mechanical buckling provide access to 3D mesostructures with applications as bio-interfaces to organoids and, by extensions, other small-scale tissue constructs for fundamental and applied study.

Supplementary Material

Refer to Web version on PubMed Central for supplementary material.

Acknowledgements

H. Ryu, Y. Park, and H. Luan equally contributed to this work. The materials and engineering efforts were supported by the Army Research Office and the Center for Bio-Integrated Electronics of the Querrey-Simpson Institute for Bioelectonics at Northwestern University. H.R. acknowledges support from the Basic Science Research Program (NRF-2019R1A6A3A12031359) through a National Research Foundation (NRF) of Korea Grant funded by the Ministry of Science and ICT. G.D. was supported by The University of Chicago Diabetes Research Center Grant P30 DK020595. Y.H. acknowledges the support from the National Science Foundation, USA (grant no. CMMI1635443). J.D.F. acknowledges support from the National Institute of Neurological Diseases and Stroke (R01NS113935, R21EB028069). K.D.J. acknowledges support from the National Institute of Neurological Diseases and Stroke (R01NS113935). This work made use of the NUFAB facility of Northwestern University's NUANCE Center, which has received support from the SHyNE Resource (NSF ECCS-1542205), the IIN, and Northwestern's MRSEC program (NSF DMR-1720139). Biological and chemical analysis was performed in the Analytical

bioNanoTechnology Core Facility of the Simpson Querrey Institute at Northwestern University. The U.S. Army Research Office, the U.S. Army Medical Research and Materiel Command, and Northwestern University provided funding to develop this facility and ongoing support is being received from the Soft and Hybrid Nanotechnology Experimental (SHyNE) Resource (NSF ECCS-1542205). Library preparation and sequencing were performed at the University of Illinois at Chicago Genome Research Core (UICGRC).

Biographies

Hanjun Ryu obtained a B.S. degree in advanced material science and engineering from the Sungkyunkwan University, South Korea in 2014. From Sungkyunkwan University, he received a Ph.D. under the supervision of Prof. Sang-Woo Kim in material science and engineering in 2019. In 2019, he joined the Rogers Research Group as a postdoctoral research fellow at the Querrey–Simpson Institute for Bioelectronics (QSIB), Center for Bio-integrated Electronics (CBIE) at Northwestern University in the United States. His research interests include transient electrical stimulators/sensors for chronic wound healing/monitoring, 3D neural interfaces for organoids analysis, and triboelectric nanogenerators for battery charging.

Yoonseok Park is a postdoctoral researcher at Querrey Simpson Institute for Bioelectronics at Northwestern University. He received his B.Sc. degree in 2006 and M.Sc. degree in 2008 from Sungkyunkwan University and Seoul National University in materials sciences and engineering and joined LG Displays in South Korea as a research engineer. After 5 years in industry, he joined TU Dresden in Germany and obtained his Ph.D. in physics in 2017. He joined the Rogers Research Group in March 2018. His research focus on the 3D neural interfaces for biological systems and biomedical and bio-inspired electronics.

Haiwen Luan obtained his B.Eng. degree (2013) in civil engineering from Tongji University, China, and M.S. degree (2015) in civil and environmental engineering and Ph.D. degree (2019) in mechanical engineering from Northwestern University. He is a postdoctoral fellow in the Querrey Simpson Institute for Bioelectronics at Northwestern University. He is interested in mechanically guided deterministic 3D assembly, and biointegrated flexible/stretchable electronics.

John Finan joined as an Assistant Professor at UIC Department of Mechanical and Industrial Engineering. He received his PhD. from Duke University and held a post-doctoral appointment at Columbia University in New York. His primary research focus is the development of human in vitro models of traumatic brain injury to enable drug discovery and patient-specific therapy in this disorder. He also develops novel tools and instruments for use with human-induced pluripotent potent stem cell-derived cells and brain organoids. His work is primarily funded by the National Institutes of Health.

John A. Rogers obtained B.A. and B.S. degrees in chemistry and in physics from the University of Texas, Austin, in 1989. From MIT, he received S.M. degrees in physics and in chemistry in 1992 and a Ph.D. in physical chemistry in 1995. After five years at Bell Laboratories, he spent thirteen years on the faculty at University of Illinois Urbana-Champaign. In 2016, he joined Northwestern University as the Louis Simpson and Kimberly Querrey Professor of Materials Science and Engineering, Biomedical Engineering and Medicine, with affiliated appointments in Mechanical Engineering, Electrical and Computer Engineering, and Chemistry. Prof. Rogers also serves as Director of the Querrey–Simpson Institute for Bioelectronics.

References

[1]. Dai X, Zhou W, Gao T, Liu J, Lieber CM, Nat. Nanotechnol 2016, 11, 776. [PubMed: 27347837]

[2]. Liu X, Yuk H, Lin S, Parada GA, Tang TC, Tham E, de la Fuente-Nunez C, Lu TK, Zhao X, Adv. Mater 2018, 30, 1704821.

[3]. Tian B, Liu J, Dvir T, Jin L, Tsui JH, Qing Q, Suo Z, Langer R, Kohane DS, Lieber CM, Nat. Mater 2012, 11, 986. [PubMed: 22922448]

[4]. Feiner R, Fleischer S, Shapira A, Kalish O, Dvir T, Control J. Release 2018, 281, 189.

[5]. Leong TG, Randall CL, Benson BR, Bassik N, Stem GM, Gracias DH, Proc. Natl. Acad. Sci. U. S. A 2009, 106, 703. [PubMed: 19139411]

[6]. Mannoor MS, Jiang Z, James T, Kong YL, Malatesta KA, Soboyejo WO, Verma N, Gracias DH, McAlpine MC, Nano Lett 2013, 13, 2634. [PubMed: 23635097]

[7]. Rijal G, Li W, Sci. Adv 2017, 3, e1700764. [PubMed: 28924608]

[8]. Park Y, Luan H, Kwon K, Zhao S, Franklin D, Wang H, Zhao H, Bai W, Kim JU, Lu W, Kim JH, Huang Y, Zhang Y, Rogers JA, Adv. Funct. Mater 2019, 29, 1903181.

[9]. Grimm D, Bof Bufon CC, Deneke C, Atkinson P, Thurmer DJ, Schaffel F, Gorantla S, Bachmatiuk A, Schmidt OG, Nano Lett 2013, 13, 213. [PubMed: 23245385]

[10]. Liu W, Chen Z, Zhou G, Sun Y, Lee HR, Liu C, Yao H, Bao Z, Cui Y, Adv. Mater 2016, 28, 3578. [PubMed: 26992146]

[11]. Liu F, Chen Y, Song H, Zhang F, Fan Z, Liu Y, Feng X, Rogers JA, Huang Y, Zhang Y, Small 2019, 15, e1804055. [PubMed: 30515973]

[12]. Yan D, Chang J, Zhang H, Liu J, Song H, Xue Z, Zhang F, Zhang Y, Nat. Commun 2020, 11, 1180. [PubMed: 32132524]

[13]. Fu H, Nan K, Bai W, Huang W, Bai K, Lu L, Zhou C, Liu Y, Liu F, Wang J, Han M, Yan Z, Luan H, Zhang Y, Zhang Y, Zhao J, Cheng X, Li M, Lee JW, Liu Y, Fang D, Li X, Huang Y, Zhang Y, Rogers JA, Nat. Mater 2018, 17, 268. [PubMed: 29379201]

[14]. Wu S-Y, Yang C, Hsu W, Lin L, Microsyst. Nanoeng 2015, 1, 2015013.

[15]. Guo SZ, Qiu K, Meng F, Park SH, McAlpine MC, Adv. Mater 2017, 29, 1701218.

[16]. Muth JT, Vogt DM, Truby RL, Menguc Y, Kolesky DB, Wood RJ, Lewis JA, Adv. Mater 2014, 26, 6307. [PubMed: 24934143]

[17]. Yang P-K, Lin Z-H, Pradel KC, Lin L, Li X, Wen X, He J-H, Wang ZL, ACS Nano 2015, 9, 901. [PubMed: 25555199]

[18]. Wang X, Jiang M, Zhou Z, Gou J, Hui D, Compos. B. Eng 2017, 110, 442.

[19]. Chen Z, Li Z, Li J, Liu C, Lao C, Fu Y, Liu C, Li Y, Wang P, He Y, J. Eur. Ceram 2019, 39, 661.

[20]. Gul JZ, Sajid M, Rehman MM, Siddiqui GU, Shah I, Kim KH, Lee JW, Choi KH, Sci. Technol. Adv. Mater 2018, 19, 243. [PubMed: 29707065]

[21]. Janbaz S, Hedayati R, Zadpoor AA, Mater. Horiz 2016, 3, 536.

[22]. Zhang Z, Demir KG, Gu GX, Int. J. Smart Nano Mater 2019, 10, 205.

[23]. Aigner TB, Haynl C, Salehi S, O'Connor A, Scheibel T, Materials Today Bio. 2020, 5, 100042.

[24]. Bertoldi K, Vitelli V, Christensen J, van Hecke M, Nat. Rev. Mater 2017, 2, 17066.

[25]. Oyefusi A, Chen J, Angew. Chem. Int. Ed. Engl 2017, 56, 8250. [PubMed: 28556408]

[26]. Ning X, Wang X, Zhang Y, Yu X, Choi D, Zheng N, Kim DS, Huang Y, Zhang Y, Rogers JA, Adv. Mater. Interfaces 2018, 5, 1800284.

[27]. Liu Y, Wang X, Xu Y, Xue Z, Zhang Y, Ning X, Cheng X, Xue Y, Lu D, Zhang Q, Zhang F, Liu J, Guo X, Hwang KC, Huang Y, Rogers JA, Zhang Y, Proc. Natl. Acad. Sci. U. S. A 2019, 116, 15368. [PubMed: 31315983]

[28]. Yan Z, Han M, Yang Y, Nan K, Luan H, Luo Y, Zhang Y, Huang Y, Rogers JA, Extreme Mech. Lett 2017, 11, 96.

[29]. Luan H, Cheng X, Wang A, Zhao S, Bai K, Wang H, Pang W, Xie Z, Li K, Zhang F, Xue Y, Huang Y, Zhang Y, ACS Appl. Mater. Interfaces 2019, 11, 3482. [PubMed: 30584766]

[30]. Lim S, Luan H, Zhao S, Lee Y, Zhang Y, Huang Y, Rogers JA, Ahn J-H, Adv. Mater 2020, 32, 2001303.

[31]. Kadoshima T, Sakaguchi H, Nakano T, Soen M, Ando S, Eiraku M, Sasai Y, Proc. Natl. Acad. Sci. U. S. A 2013, 110, 20284. [PubMed: 24277810]

[32]. Lancaster MA, Renner M, Martin CA, Wenzel D, Bicknell LS, Hurles ME, Homfray T, Penninger JM, Jackson AP, Knoblich JA, Nature 2013, 501, 373. [PubMed: 23995685]

[33]. Di Carlo D, J. Lab. Autom 2012, 17, 32. [PubMed: 22357606]

[34]. Karzbrun E, Kshirsagar A, Cohen SR, Hanna JH, Reiner O, Nat. Phys 2018, 14, 515. [PubMed: 29760764]

[35]. Alcaraz J, Xu R, Mori H, Nelson CM, Mroue R, Spencer VA, Brownfield D, Radisky DC, Bustamante C, Bissell MJ, EMBO J 2008, 27, 2829. [PubMed: 18843297]

[36]. Achberger K, Probst C, Haderspeck J, Bolz S, Rogal J, Chuchuy J, Nikolova M, Cora V, Antkowiak L, Haq W, Shen N, Schenke-Layland K, Ueffing M, Liebau S, Loskill P, Elife 2019, 8, e46188. [PubMed: 31451149]

[37]. Brandenberg N, Hoehnel S, Kuttler F, Homicsko K, Ceroni C, Ringel T, Gjorevski N, Schwank G, Coukos G, Turcatti G, Lutolf MP, Nat. Biomed. Eng 2020, 4, 863. [PubMed: 32514094]

[38]. Decembrini S, Hoehnel S, Brandenberg N, Arsenijevic Y, Lutolf MP, Sci. Rep 2020, 10, 10275. [PubMed: 32581233]

[39]. Lancaster MA, Knoblich JA, Nat. Protoc 2014, 9, 2329. [PubMed: 25188634]

[40]. von Metzen RP, Stieglitz T, Biomed. Microdevices 2013, 15, 727. [PubMed: 23494595]

[41]. Wright RM, Ramesh KT, Biomech. Model. Mechanobiol 2012, 11, 245. [PubMed: 21476072]

[42]. Hertz H, J. Reine Angew. Math 1882, 92, 156–171.

[43]. Rheinlaender J, Dimitracopoulos A, Wallmeyer B, Kronenberg NM, Chalut KJ, Gather MC, Betz T, Charras G, Franze K, Nat. Mater 2020, 19, 1019. [PubMed: 32451510]

[44]. Budday S, Nay R, de Rooij R, Steinmann P, Wyrobek T, Ovaert TC, Kuhl E, J. Mech. Behav. Biomed. Mater 2015, 46, 318. [PubMed: 25819199]

[45]. Antonovaite N, Beekmans SV, Hol EM, Wadman WJ, Iannuzzi D, Sci. Rep 2018, 8, 12517. [PubMed: 30131608]

[46]. Guz N, Dokukin M, Kalaparthi V, Sokolov I, Biophys. J 2014, 107, 564. [PubMed: 25099796]

[47]. Efremov YM, Okajima T, Raman A, Soft Matter 2020, 16, 64. [PubMed: 31720656]

[48]. Sales A, Holle AW, Kemkemer R, Soft Matter 2017, 13, 5158. [PubMed: 28664962]

[49]. Zhu Y, Wang L, Yin F, Yu Y, Wang Y, Shepard MJ, Zhuang Z, Qin J, Integr. Biol. (Camb.) 2017, 9, 968. [PubMed: 29168871]

[50]. Rauscher AA, Gyimesi M, Kovacs M, Malnasi-Csizmadia A, Trends Biochem. Sci 2018, 43, 700. [PubMed: 30057142]

[51]. Petrosyan A, Casey CA, Cheng PW, Sci. Rep 2016, 6, 31962. [PubMed: 27535804]

[52]. Haorah J, Heilman D, Knipe B, Chrastil J, Leibhart J, Ghorpade A, Miller DW, Persidsky Y, Alcohol. Clin. Exp. Res 2005, 29, 999. [PubMed: 15976526]

[53]. Martens JC, Radmacher M, Pflugers Arch 2008, 456, 95. [PubMed: 18231808]

[54]. Dominijanni A, Devarasetty M, Soker S, iScience 2020, 23, 101851. [PubMed: 33319176]

[55]. Park Y, Franz CK, Ryu H, Luan H, Cotton KY, Kim JU, Chung TS, Zhao S, Vazquez-Guardado A, Yang DS, Li K, Avila R, Phillips JK, Quezada MJ, Jang H, Kwak SS, Won SM, Kwon K, Jeong H, Bandodkar AJ, Han M, Zhao H, Osher GR, Wang H, Lee K, Zhang Y, Huang Y, Finan JD, Rogers JA, Sci. Adv 2021, 7, eabf9153. [PubMed: 33731359]

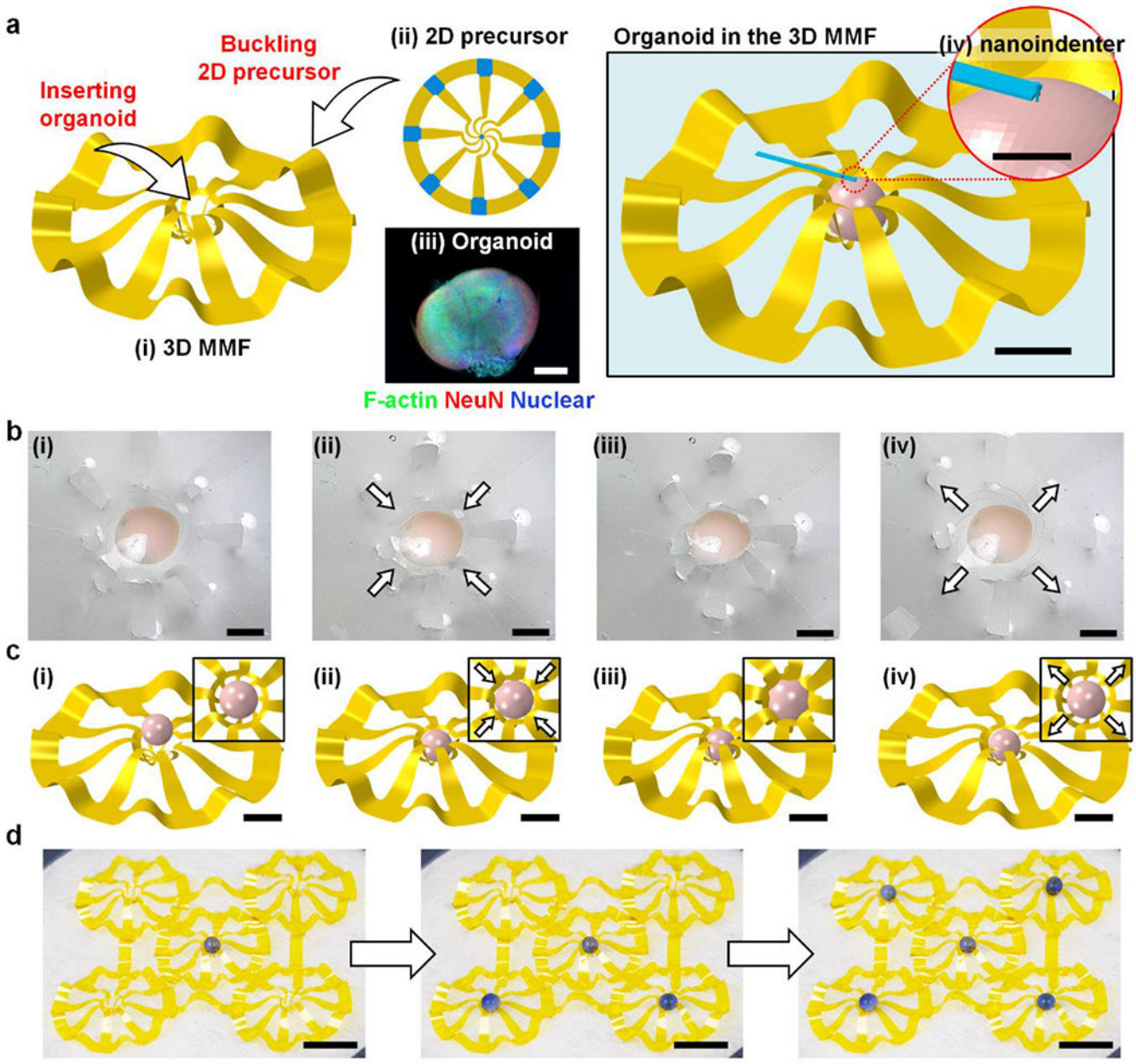

Figure 1.

(**a**) Schematic image of an organoid in the 3D MMF. scale bar: 2 mm. (i) 3D MMF after buckling (ii) 2D precursor, with bonding sites indicated in blue. (iii) Immunohistochemistry for F-actin (green), NeuN (red), and Nuclear (blue) in a cerebral organoid. scale bar: 0.5 mm. (iv) Location of nanoindenter on an organoid for indentation. scale bar: 0.5 mm. (**b**) Optical micrographs of the reversible close and open process of the 3D MMF. (i) the opened 3D MMF with an organoid, (ii) releasing the substrate to close, (iii) fully closed withhold the organoid, (iv) the opened 3D MMF after stretching the substrate. scale bar: 1 mm. (**c**) FEA results at different stages of the process of inserting the cerebral organoid into the 3D MMF; from left (i) slightly stretch the substrate to open the 3D MMF and insert organoid

(ε_{appl} = 10 %), (ii) slightly releasing the substrate to close 3D MMF (ε_{appl} = 5 %), (iii) fully release the substrate to close the 3D MMF (ε_{appl} = 0 %), and (iv) slightly stretch the substrate to open the 3D MMF and remove organoid (ε_{appl} = 10 %). scale bar: 2 mm. Inset figures are top view images of corresponding FEA results. (**d**) Arrays of 3D MMFs with similar dimensions, for high throughput screening; (from left) after inserting a single sphere into the center 3D MMF, after inserting two additional spheres in the bottom pair of 3D MMFs, and after inserting two additional spheres in the top pair of 3D MMFs. scale bar: 2 cm.

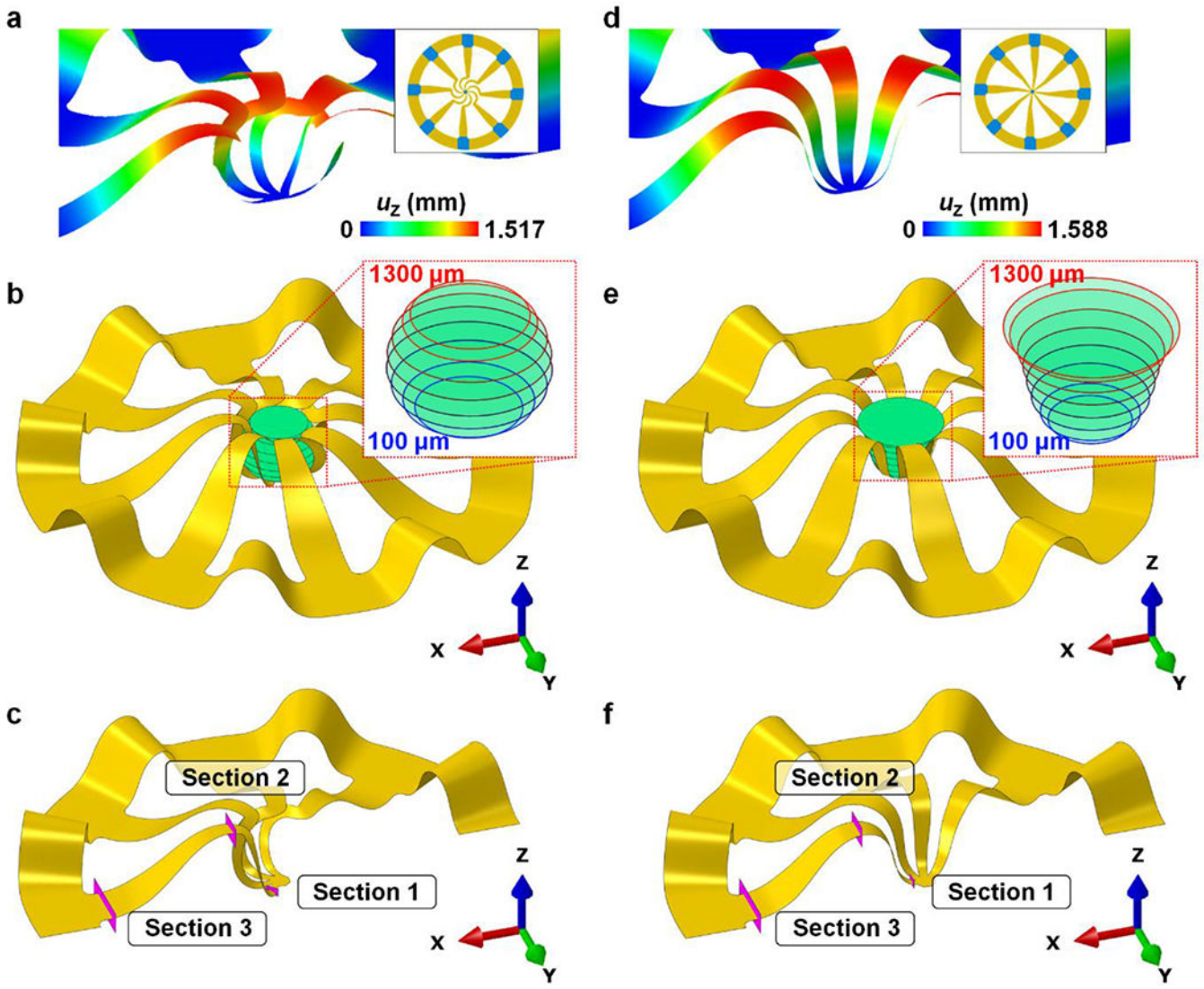

Figure 2.

FEA results of geometries and out-of-plane displacements (u_z) associated with 3D MMFs with (**a**) twisted and (**d**) straight designs. The insets show the layouts of the 2D precursors, with bonding sites indicated in blue. The sectional diameters of the spaces defined by these structures at eight different heights for the (**b**) twisted and (**e**) straight designs. Illustration of the locations for reported bending stiffnesses for the (**c**) twisted and (**f**) straight designs.

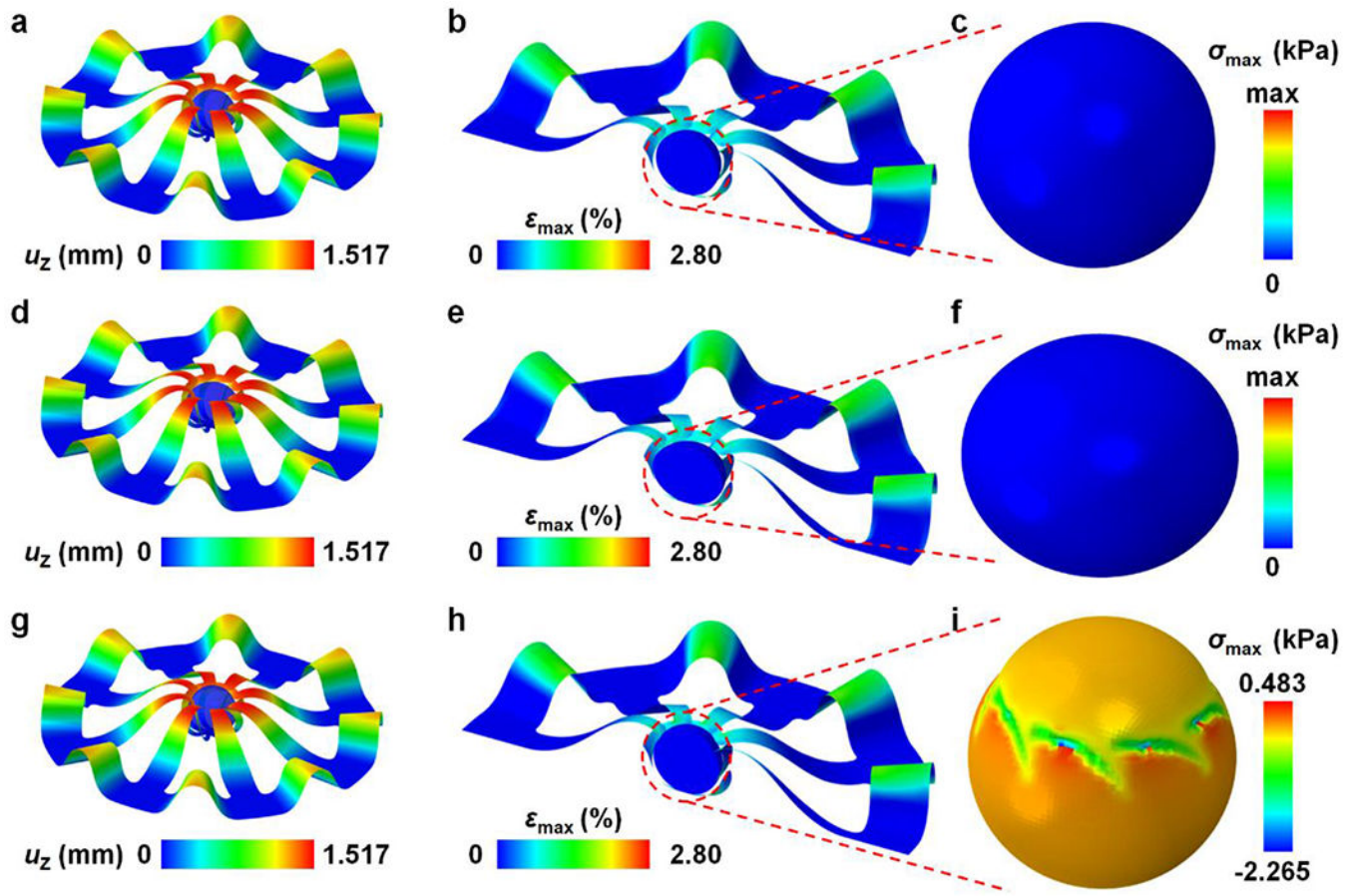

Figure 3.

FEA results for the out-of-plane displacements (u_z), and the distribution of strains and stresses of 3D MMFs enclosing (**a-c**) a 1.6 mm diameter spherical organoid, (**d-f**) an ellipsoidal organoid (a = 0.9 mm, b = 0.9 mm, c = 0.75 mm), and (**g-i**) a 1.7 mm diameter spherical organoid.

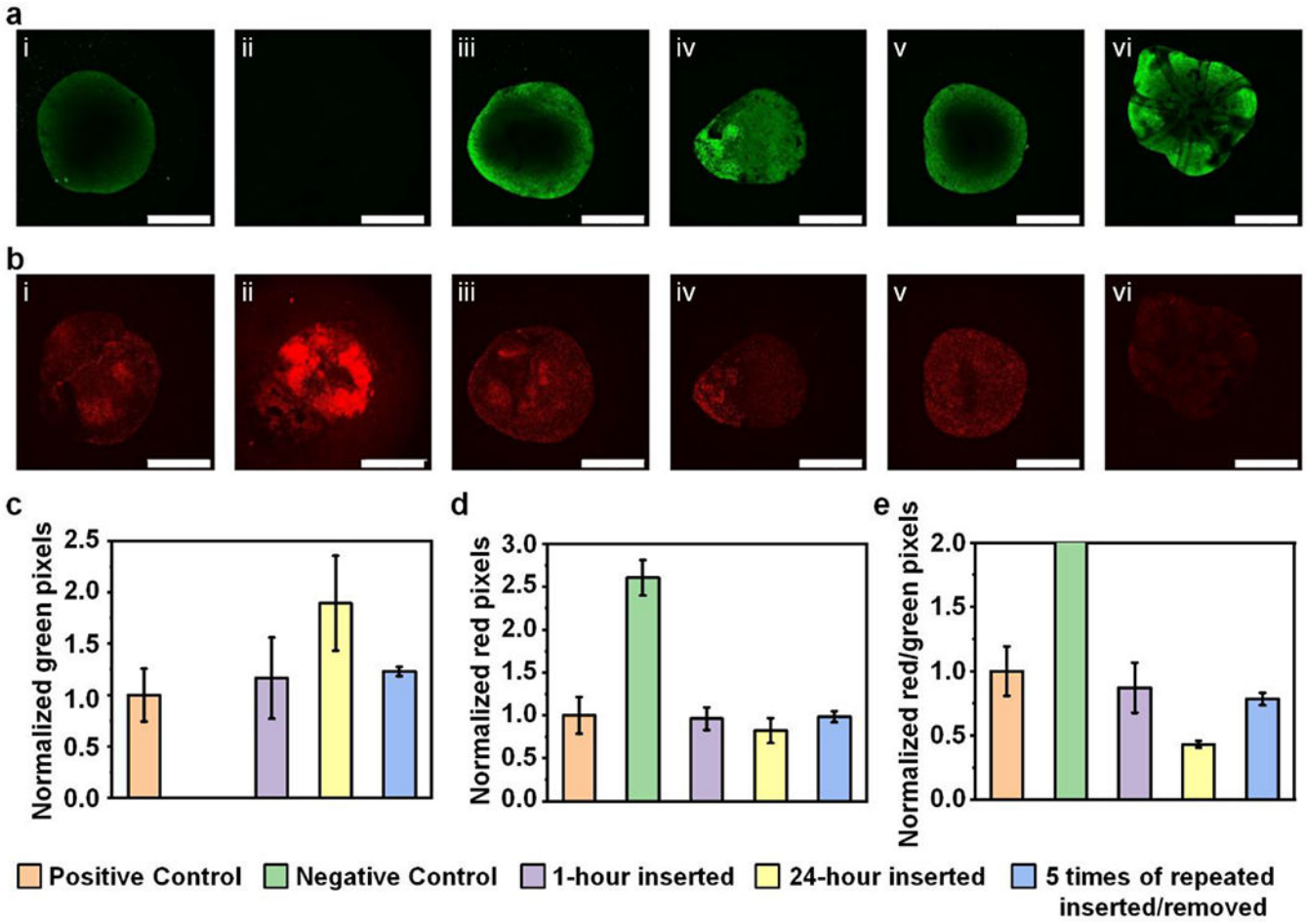

Figure 4.

(**a**) Calcein AM and (**b**) propidium iodide stained fluorescence images of organoids associated with (i) a positive control, in the form of an organoid not in a 3D MMF, (ii) a negative control, in the form of an organoid exposed to a toxic drug, (iii) an organoid one hour after insertion into a 3D MMF followed by removal, (iv) an organoid 24 hours after insertion into a 3D MMF followed by removal, (v) an organoid after five cycles of insertion and removal from a 3D MMF, and vi) an organoid 24 hours after insertion into a 3D MMF, while still in the 3D MMF. scale bar: 1 mm, 164-day aged organoids. Normalized numbers of pixels for (c) Calcein AM (green) and (d) PI (red), and for (e) ratios of PI and Calcein AM. n=3, 164-day aged organoids. Error bars correspond to standard deviations.

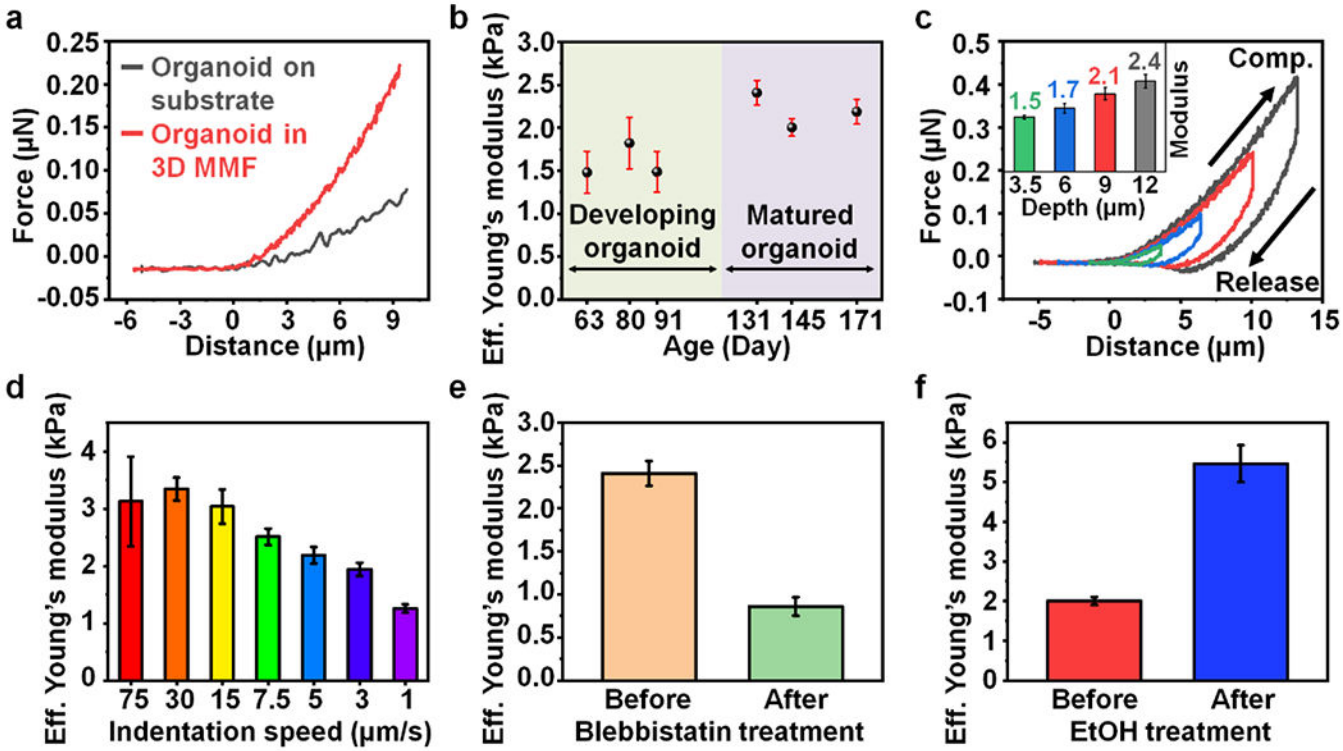

Figure 5.

(**a**) Force-distance curves and effective Young's modulus of organoids and the 3D MMF. (**b**) Effective Young's modulus of different ages organoids measured in a 3D MMF with an indentation speed of 5 μm/s. (**c**) Force-distance curves for indentation depths of 3.5, 6, 9, and 12 μm at speeds of 5 μm/s. The inset graph shows the effective Young's modulus from data collected to depths of 3.5 (green), 6 (blue), 9 (red), and 12 μm (black). (**d**) Effective Young's modulus values determined at different indentation speeds to depths of 12 μm. Effective Young's modulus values before and after (**e**) exposure to blebbistatin (10 μM) for 2-hours and (**f**) exposure to ethanol (50 mM) for 2-hours. Error bars correspond to one standard deviation. A number of indentations : >15.

Table 1.

Effect of inserting an organoid into a 3D MMF on gene expression, using 18S as the reference gene. Statistical significance was calculated using the Benjamini-Hochberg procedure.

Gene	Type	Fold Change due to Insertion	P-value
18S	Selected Control	1	
FOXG1	Target	1.0932	0.7865
RBFOX3/NEUN	Target	2.6647	0.0016
RPL37A	Candidate Control	1.0864	0.4111
S100B	Target	0.2605	0.0926
TUJ1/TUBB3	Target	1.6746	0.0926

Table 2.

Effect of inserting an organoid into a 3D MMF on gene expression, using RPL37A as the reference gene. Statistical significance was calculated using the Benjamini-Hochberg procedure.

Gene	Type	Fold Change due to Insertion	P-value
18S	Candidate Control	0.9099	0.4121
FOXG1	Target	0.9683	0.9385
RBFOX3/NEUN	Target	2.368	0.0194
RPL37A	Selected Control	1	
S100B	Target	0.2244	0.2383
TUJ1/TUBB3	Target	1.4489	0.3524